ChemPubSoc Europe

DOI: 10.1002/chem.201302461

CHEMISTRY A European Journal Full Paper

Sensors

Chromo-Fluorogenic Detection of Nitroaromatic Explosives by Using Silica Mesoporous Supports Gated with Tetrathiafulvalene Derivatives

Yolanda Salinas,[a, b] Marta V. Solano,[c] Rebecca E. Sørensen,[c] Karina R. Larsen,[c] Jess Lycoops,[c] Jan O. Jeppesen,*[c] Ramón Martínez-Máñez,*[a, b] Félix Sancenón,[a, b] M. Dolores Marcos,[a, b] Pedro Amorós,[d] and Carmen Guillem[d]

Abstract: Three new hybrid gated mesoporous materials (**SN_3-1**, **SNH_2-2**, and **SN_3-3**) loaded with the dye $[Ru(bipy)_3]^{2+}$ (bipy = bipyridine) and capped with different tetrathiafulvalene (TTF) derivatives (having different sizes and shapes and incorporating different numbers of sulfur atoms) have been prepared. The materials **SN_3-1** and **SN_3-3** are functionalized on their external surfaces with the TTF derivatives **1** and **3**, respectively, which were attached by employing the "click" chemistry reaction, whereas **SNH_2-2** incorporates the TTF derivative **2**, which was anchored to the solid through an amidation reaction. The final gated materials have been characterized by standard techniques. Suspensions of these solids in acetonitrile showed "zero release", most likely because of the formation of dense TTF networks around the pore outlets. The release of the entrapped $[Ru(bipy)_3]^{2+}$ dye from **SN_3-1**, **SNH_2-2**, and **SN_3-3** was studied in the presence of selected explosives (Tetryl, TNT, TNB, DNT, RDX, PETN, PA, and TATP). **SNH_2-2** showed a fairly selective response to Tetryl, whereas for **SN_3-1** and **SN_3-3** dye release was found to occur with Tetryl, TNT, and TNB. The uncapping process in the three materials can be ascribed to the formation of charge-transfer complexes between the electron-donating TTF units and the electron-accepting nitroaromatic explosives. Finally, solids **SNH_2-2** and **SN_3-1** have been tested for Tetryl detection in soil with good results, pointing toward a possible use of these or similar hybrid capped materials as probes for the selective chromo-fluorogenic detection of nitroaromatic explosives.

Introduction

The indiscriminate use of explosives in terrorist attacks in the last few years has increased attention on the design of new probes for the reliable and accurate detection of these lethal chemicals. In this field, and taking into account the widespread use of explosive formulations, the analysis of explosives is of relevant interest in forensic research, landmine detection, and in the study of environmental problems associated with their residues.[1]

Explosive compounds, depending on their chemical nature, are classified into four classes, namely (i) nitroaromatics and nitroalkanes, (ii) nitramines, (iii) nitrate esters, and (iv) peroxides.[2] Among these classes, nitroaromatics are perhaps the most widely used in criminal acts, in landmines, and in cluster bombs. Nitroaromatic explosives are molecules composed of a benzene ring functionalized with several nitro groups. Nitroaromatic explosives are electron deficient in nature on account of the presence of the electron-withdrawing nitro moieties, which lower the energy of the empty π^* orbital, thereby making them good electron acceptors.[3]

Standard methodologies for the detection and quantification of explosives involve, among others, the use of trained canine teams,[4] gas chromatography coupled with mass spectrometry,[5] gas chromatography–electron capture detection,[6] surface-enhanced Raman spectroscopy,[7] mass spectrometry,[8] X-ray imaging,[9] thermal neutron analysis,[10] electrochemical procedures,[11] and ion mobility spectroscopy (IMS).[12] The above mentioned methods offer several advantages, but some of them also have drawbacks related to a lack of portability (for "in situ" detection), susceptibility to false positives owing to environmental contaminants, or false negative readings on account of interfering compounds. In this context, the use of

[a] Dr. Y. Salinas, Prof. R. Martínez-Máñez, Dr. F. Sancenón, Dr. M. D. Marcos
Centro de Reconocimiento Molecular y Desarrollo Tecnológico (IDM)
Unidad mixta Universidad Politécnica de Valencia-Universidad de Valencia
Departamento de Química, Universidad Politécnica de Valencia
Camino de Vera s/n, 46022 Valencia (Spain)
E-mail: rmaez@qim.upv.es

[b] Dr. Y. Salinas, Prof. R. Martínez-Máñez, Dr. F. Sancenón, Dr. M. D. Marcos
CIBER de Bioingeniería, Biomateriales y Nanomedicina (CIBER-BBN)

[c] Dr. M. V. Solano, R. E. Sørensen, Dr. K. R. Larsen, Dr. J. Lycoops, Prof. J. O. Jeppesen
Department of Physics, Chemistry, and Pharmacy
University of Southern Denmark Campusvej 55, 5230 Odense M (Denmark)
E-mail: joj@sdu.dk

[d] Prof. P. Amorós, Dr. C. Guillem
Institut de Ciència del Materials (ICMUV)
Universitat de València
P.O. Box 2085, 46071 Valencia (Spain)

Supporting information for this article is available on the WWW under http://dx.doi.org/10.1002/chem.201302461.

chromo-fluorogenic chemosensors based on supramolecular assemblies has been explored for the detection of explosives.[13] In such molecular probes, interaction with the explosive induces changes in color or in fluorescence that are easily measurable. Based on this simple concept, chemosensors for the optical detection of explosives based on various functionalized dye molecules have been reported.[14] Most of these probes have been reliant on the electron-deficient character of nitroaromatic explosives, as a result of which they form π-stacking charge-transfer complexes with electron-donating molecules.[15] However, a common drawback of these probes is that fluorescence quenching is usually observed because of the occurrence of electron-transfer processes between the corresponding excited fluorophore and the nitroaromatic explosive. Probes that exhibit a *turn-on* response rather than *turn-off* behavior would be preferable but, to the best of our knowledge, only a few examples of probes showing a *turn-on* response to nitroaromatic explosives have hitherto been reported in the literature.[16]

Polycyclic aromatic hydrocarbons have been extensively used as electron-rich molecules in the development of fluorogenic probes for the detection of nitroaromatic explosives.[17] Other electron-rich molecules that merit attention are tetrathiafulvalenes (TTF). The huge potential of TTF derivatives was first established by the discovery of their conductive behavior.[18] Since then, other properties of the TTF unit, such as its electro-active character and its strong π-donating nature, have also been exploited.[19] Utilizing the latter property, TTF moieties have recently been incorporated into calixarenes and other supramolecular frameworks in order to prepare chemosensors for nitroaromatic explosives.[20]

From another point of view, the blending of supramolecular assemblies and inorganic materials has recently resulted in the preparation of gated materials.[21] These are systems in which the release of an entrapped cargo can be controlled on-command through the use of selected external stimuli that control the state of the gate (open or closed).[22] These gated materials usually consist of two components: i) a switchable gate-like ensemble, and ii) a suitable inorganic support serving as a nanocontainer, on which the gate-like system is grafted. Mesoporous silica materials with different pore sizes and morphologies have been selected for use as inorganic scaffolds in the preparation of gated ensembles. These supports have large surface areas (up to 1200 $m^2 g^{-1}$), large load capacities, are chemically inert, and are easy to functionalize through the use of established alkoxysilane chemistry.[23] As regards the gate-like ensemble, several molecular, supramolecular, and nanoscopic systems have been used. Moreover, opening of the gate and cargo delivery has been accomplished by means of several physical,[24] chemical,[25] and biochemical[26] triggers. Although most of the reported gated materials have been designed for drug-delivery applications, some recent examples have concerned the use of capped mesoporous particles for sensing.[27] The underlying concept here is that interaction of a target analyte with the gated ensemble controls the release of the cargo (a dye), resulting in a chromo-fluorogenic signal.[28] This novel approach is highly modular and displays potential for the development of novel signaling systems through the selection of different inorganic porous supports, diverse guest-selective gate-like ensembles, and a wide range of dyes and fluorophores. In addition, this approach separates the recognition protocol (binding site–analyte interaction) from the signaling event, making sensing independent of the stoichiometry of the host–guest complex and sometimes giving rise to signal amplification.[29]

Following this approach, in a seminal work, polyamine-functionalized mesoporous materials were used for the selective detection of ATP through interaction of this bulky anion with the polyamines, which resulted in an inhibition of dye release.[27a] Inhibition of dye release by coordination of target analytes to binding sites on mesoporous supports has also been used to prepare hybrid materials capable of selectively detecting long-chain carboxylates[27b] (through electrostatic interactions with grafted imidazolium cations) and borates[27c] (through the formation of borate esters with grafted saccharides). In another group of examples, the gated materials remain closed until the interaction of a target analyte triggers the release of the entrapped dye. Following this approach, DNA-capped mesoporous materials have been used to detect the presence of complementary DNA strands[27d] and for the detection of *Mycoplasma*,[27e] mercury,[27f] and telomerase activity.[27g] Selective aptamers have also been used as caps for the preparation of a hybrid material for the detection of α-thrombin in human plasma.[27h] Similar sensing systems have been developed based on antibody-capped mesoporous supports that can be selectively opened in the presence of the corresponding antigen. Using this approach, hybrid sensory materials for the detection of sulfathiazole,[27i] finasteride,[27j] and TATP[27k] have been described. Moreover, small molecules, such as methylmercury, have also been chromo-fluorogenically detected through a pore-opening protocol based on hybrid materials capped with bulky thiol-containing organic moieties.[29]

Bearing in mind these independent concepts and following our interest in the preparation of new probes for the detection of explosives[16] and the design of new applications for capped mesoporous materials,[30] we report herein the synthesis and signaling behavior toward nitroaromatic explosives of three gated mesoporous supports decorated on their external surfaces with three different π-electron-donating TTF derivatives (Scheme 1) and loaded with a dye (e.g., $[Ru(bipy)_3]^{2+}$). The prepared nanoprobes were designed to show "zero release" because of the formation of a dense network of TTF units around the pores. The signaling protocol (Scheme 1) relies on interaction between electron-deficient nitroaromatic explosives and the strongly π-electron-donating TTF moieties, which results in rupture of the TTF–TTF interactions allowing release of the entrapped dye. It is demonstrated that this approach leads to relatively simple hybrid probes for nitroaromatic explosives capable of showing a *turn-on* response, in contrast to the widely observed *turn-off* behavior shown by probes based on single molecules or fluorophore-containing polymers.[16]

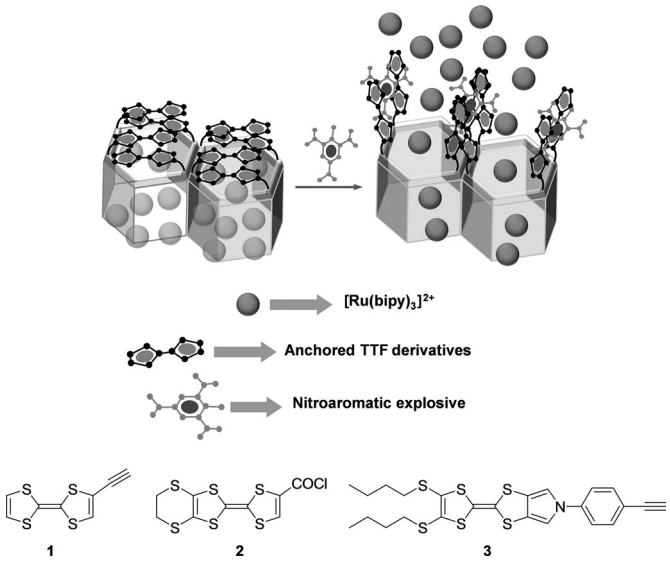

Scheme 1. Top: Schematic representation of the sensory hybrid mesoporous materials and the uncapping mechanism in the presence of nitroaromatic explosives. Bottom: The structures of the TTF derivatives (**1**, **2**, and **3**) used for surface functionalization.

Results and Discussion

The gated material

The prepared hybrid solids are schematically illustrated in Scheme 2. The MCM-41 mesoporous support was prepared according to a well-known procedure from tetraethyl orthosilicate (TEOS) as an inorganic precursor and *n*-cetyltrimethylammonium bromide (CTAB) as a porogenic species.[31] The surfactant was removed by calcination to obtain the final MCM-41 starting material. The solid was then loaded with $[Ru(bipy)_3]^{2+}$ as a suitable fluorophore, and the outer surface was functionalized with 3-(azidopropyl)triethoxysilane groups (giving $\mathbf{SN_3}$, for the further preparation of the sensing materials $\mathbf{SN_3}$**-1** and $\mathbf{SN_3}$**-3**) or with 3-(aminopropyl)triethoxysilane groups (giving $\mathbf{SNH_2}$, for the preparation of the sensing support $\mathbf{SNH_2}$**-2**). By this grafting procedure, the silane groups were preferentially attached to the external surface rather than to the inside of the mesopores, which contained the $[Ru(bipy)_3]^{2+}$ dye. In the second step (Scheme 2), the TTF derivatives **1** or **3**, both bearing an alkyne moiety, were attached to the outer surface of the solid $\mathbf{SN_3}$ by a copper(I)-catalyzed Huisgen azide/alkyne 1,3-dipolar cycloaddition "click" reaction.[32] This led to the formation of a 1,2,3-triazole heterocycle and yielded the final hybrid materials $\mathbf{SN_3}$**-1** and $\mathbf{SN_3}$**-3**, respectively. The resulting solids were collected by filtration, extensively washed with water and with organic solvents, before being dried overnight at 36 °C. Water washings were carried out in order to remove possible traces of copper from the surfaces of the final solids. For the preparation of $\mathbf{SNH_2}$**-2**, the solid $\mathbf{SNH_2}$ was reacted with the acyl chloride derivative **2** in acetonitrile/K_2CO_3 in order to attach the TTF derivative through an amide linkage (Scheme 2). After completion of the reaction, the final sensing material was collected by filtration and extensively washed, before being dried overnight at 36 °C.

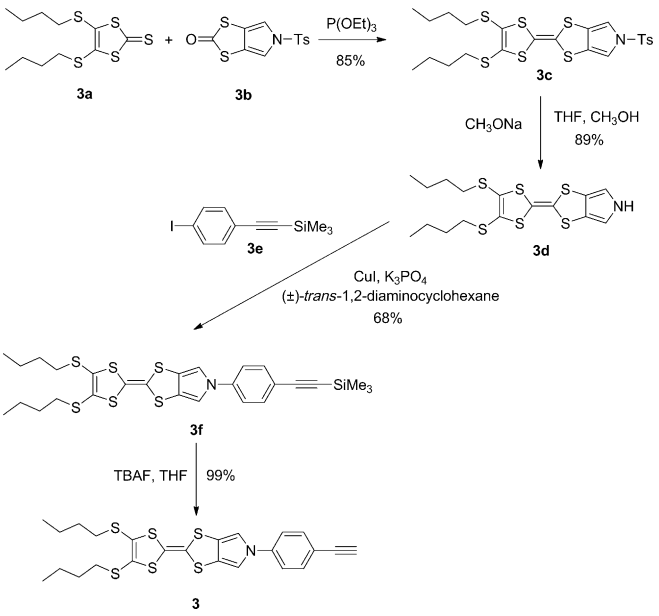

Scheme 3. Synthetic route for the preparation of compound **3**. Ts = tosyl, TBAF = tetra-*n*-butylammonium fluoride.

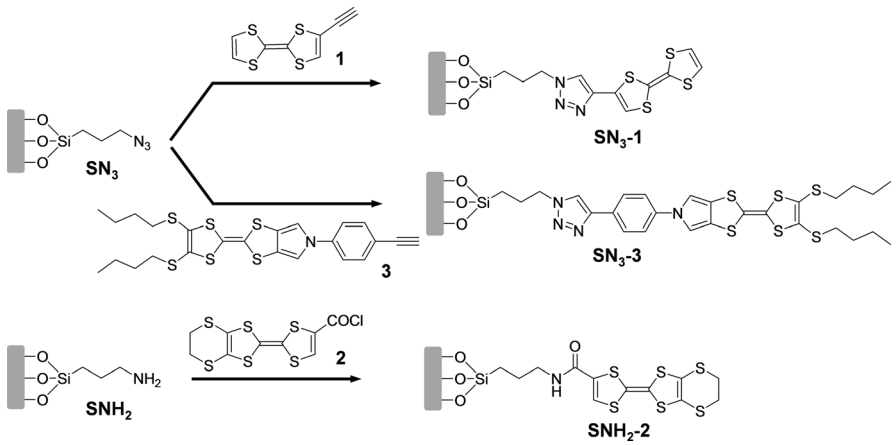

Scheme 2. Synthetic routes for the preparation of solids $\mathbf{SN_3}$**-1**, $\mathbf{SNH_2}$**-2**, and $\mathbf{SN_3}$**-3**.

The TTF derivatives **1**[33] and **2**[34] were prepared according to literature procedures, whereas the novel TTF derivative **3** was synthesized by a four-step procedure as depicted in Scheme 3. The synthesis of **3** involved an initial cross-coupling of 4,5-bis-(butylthio)-1,3-dithiole-2-thione (**3a**)[35] with *N*-tosyl-1,3-dithiolo-[4,5-*c*]pyrrole-2-one (**3b**)[36] in refluxing triethyl phosphite, which afforded the TTF derivative **3c** in 85% yield. The tosyl protecting group in **3c** was then removed

by treatment with sodium methoxide in THF/methanol to afford compound **3d** (89% yield). The third step was a microwave-assisted coupling between **3d** and (4-iodophenylethynyl)trimethylsilane (**3e**) catalyzed by CuI, which afforded the TTF derivative **3f** in 68% yield. Finally, the alkynyl-TTF derivative **3** was obtained in almost quantitative yield by deprotection[37] of the TMS group using tetra-*n*-butylammonium fluoride (TBAF).

Characterization of the materials

The starting MCM-41 and the final solid sensing materials **SN_3-1**, **SNH_2-2**, and **SN_3-3** were characterized by conventional solid-state procedures. The mesoporous structure of the MCM-41 material was confirmed by powder X-ray diffraction (PXRD) and transmission electron microscopy (TEM) techniques. Figure 1 shows the PXRD patterns of the as-synthesized MCM-41, calcined MCM-41, and the final supports **SN_3-1**, **SNH_2-2**, and **SN_3-3**. The PXRD pattern of siliceous as-synthesized MCM-41 shows four low-angle reflections typical of a hexagonal ordered array, which can be indexed as (100), (110), (200), and (210) Bragg peaks. A shift of the (100) reflection and a remarkable broadening of the (110) and (200) peaks was observed in the PXRD pattern of the calcined MCM-41. This corresponds to an approximate cell contraction of 6–8 Å during the calcination step. Despite this partial loss of order, the fact that the overlapped (100), (110), and (200) reflections were still observed indicated that the mesopore symmetry was preserved after calcination. The PXRD patterns of the final capped solids (**SN_3-1**, **SNH_2-2**, and **SN_3-3**) only displayed the (100) reflection. For these solids, peaks (110) and (200) were lost, which was most probably due to reduced contrast arising from the filling of the pore voids by the ruthenium complex. Nevertheless, the clear presence of the (100) peak in these patterns indicated that the loading and functionalization process did not substantially modify the mesoporous structure of the final supports.

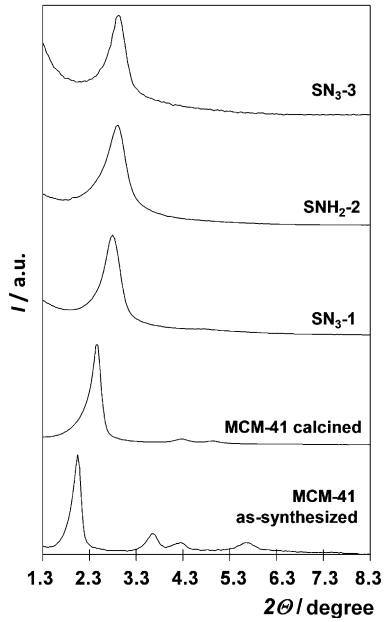

Figure 1. Small-angle PXRD patterns of as-synthesized MCM-41, calcined MCM-41, and the final solids **SN_3-1**, **SNH_2-2**, and **SN_3-3**.

The presence of the mesoporous structure in the final functionalized solids was also confirmed by TEM analysis, in which the typical channels of the MCM-41 matrix were seen as black and white stripes (Figure 2). TEM images also showed that the final solids were obtained as microparticles. SEM analysis by energy-dispersive X-ray spectroscopy (EDX, 20 kV) did not show any characteristic signal for Cu, indicating that no residual Cu from the "click" reaction was present on the final isolated **SN_3-1** and **SN_3-3** materials. Moreover, the EDX analysis clearly indicated the presence of sulfur atoms (due to grafted TTF moieties) in **SN_3-1**, **SN_3-3**, and **SNH_2-2**.

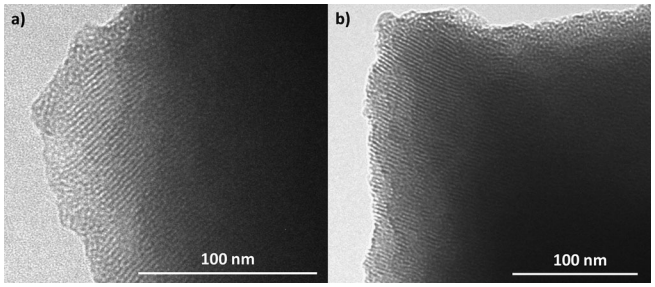

Figure 2. TEM images of a) calcined MCM-41 and b) the final solid **SNH_2-2** showing the typical porosity of the MCM-41 matrix.

N_2 adsorption–desorption studies of the calcined MCM-41, **SN_3-1**, **SNH_2-2**, and **SN_3-3** materials were also carried out. Figure 3 shows the nitrogen adsorption–desorption isotherms obtained for calcined MCM-41, **SNH_2**, and **SNH_2-2**. The calcined MCM-41 showed a typical curve for a mesoporous support, consisting of an adsorption step at an intermediate P/P_0 values (0.1–0.3). These isotherms could be classified as type IV, characteristic of mesoporous materials in which the observed step relates to nitrogen condensation inside the mesopores. The pore

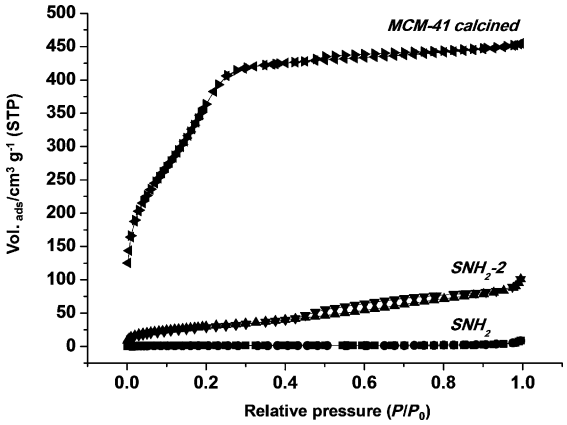

Figure 3. Nitrogen adsorption–desorption isotherms for calcined MCM-41, **SNH_2**, and **SNH_2-2**. STP = standard temperature and pressure.

size distributions (PSD) of these samples were calculated by employing the Barrett–Joyner–Halenda (BJH) method.[38] The pore diameters estimated from analysis of the respective TEM images were in agreement with these values. The narrow BJH pore size distribution and the absence of a hysteresis loop in this interval pointed to the existence of uniform cylindrical mesopores (pore diameter 2.25 nm and pore volume 0.45 $cm^3 g^{-1}$, calculated by using the BJH model on the adsorption branch of the isotherm). Application of the Brunauer–Emmett–Teller (BET) model[39] resulted in a value of 1036.2 $m^2 g^{-1}$ for the total specific surface area. From the PXRD pattern, porosimetry, and TEM studies, the a_0 cell parameter (3.65 nm) and the wall thickness (1.4 nm) were obtained.

The N_2 adsorption–desorption isotherms of solids **SN_3**, **SNH_2**, **SN_3-1**, **SNH_2-2**, and **SN_3-3** were typical of mesoporous systems with partially filled mesopores, and decreases in the N_2 volume adsorbed and specific surface area were observed (see Table 1). This was especially pronounced for the solids **SN_3**, **SNH_2**, **SNH_2-2**, and **SN_3-3**, whereas for solid **SN_3-1** a relatively high specific surface area was still observed. The reduction in the BET surface area compared with that of the MCM-41 starting material can be attributed to the loading of the pores with the ruthenium(II) complex and the functionalization of the surface silanol groups with bulky TTF moieties.[40]

Table 1. BET specific surface areas, pore volumes, and pore sizes calculated from the N_2 adsorption–desorption isotherms.

Sample	S_{BET} [$m^2 g^{-1}$]	BJH Pore Size[a,b] [nm]	Total Pore Volume[a] [$cm^3 g^{-1}$]
MCM-41	1036.2	2.25	0.45
SN_3	77.9	<2	0.03
SNH_2	50.2	<2	0.01
SN_3-1	816.2	2.27	0.37
SN_3-3	558.0	2.61	0.27
SNH_2-2	111.4	<2	0.15

[a] Pore volumes and pore sizes relate only to intraparticle mesopores. [b] Pore size estimated by the BJH model applied to the adsorption branch of the isotherm.

The contents of the $[Ru(bipy)_3]^{2+}$ complex and the TTF derivatives in the solids were determined by thermogravimetric analysis, EDX, and elemental analysis (see Table 2). The thermogravimetric traces for **SN_3-1**, **SNH_2-2**, and **SN_3-3** showed three weight loss steps ($T < 210\,^{\circ}C$, $210\,^{\circ}C < T < 800\,^{\circ}C$, $T > 800\,^{\circ}C$) related to solvent elimination (11.77%, 8.23%, and 15.49% for **SN_3-1**, **SNH_2-2**, and **SN_3-3**, respectively), decomposition of grafted organic groups and of the ruthenium complex (11.66%, 31.06%, and 12.13% for **SN_3-1**, **SNH_2-2**, and **SN_3-3**, respectively) and, finally, condensation of silanol groups on the siliceous surface (0.93%, 1.18%, and 1.17% for **SN_3-1**, **SNH_2-2**, and **SN_3-3**, respectively).

Table 2. Content (α) of anchored molecules and dye in mmol g^{-1} of SiO_2.

Solid	α_{amine}	α_{azide}	α_{dye}	α_{TTF}
SN_3	–	0.65	0.53	–
SN_3-1	–	–	0.04	0.29
SN_3-3	–	–	0.14	0.10
SNH_2	0.73	–	0.55	–
SNH_2-2	–	–	0.52	0.42

From the data in Tables 1 and 2, the specific surface areas of the final solids were clearly correlated to the dye contents in the porous networks. For instance, solid **SN_3-1** had a higher specific surface area (816.2 $m^2 g^{-1}$) than that of **SNH_2-2** (111.4 $m^2 g^{-1}$), which correlates well with the lower ruthenium(II) content found for the former.

In addition, the data in Table 2 also indicate that functionalization with the TTF derivatives on the azide- and amine-functionalized solids **SN_3** and **SNH_2** was incomplete. We calculated that around 44% and 15% of the anchored azide groups on **SN_3** had been functionalized with the TTF derivatives **1** and **3** in solids **SN_3-1** and **SN_3-3**, respectively, and that around 57% of the anchored amine groups on **SNH_2** had reacted with the TTF derivative **2**.

^{29}Si NMR spectroscopic studies on the solids **SNH_2** and **SNH_2-2** as well as the starting MCM-41 confirmed the anchoring of the organosilane groups (see Figure 4 and Table 3). A relative decrease in the amount of Q^2+Q^3 (silanol) sites in

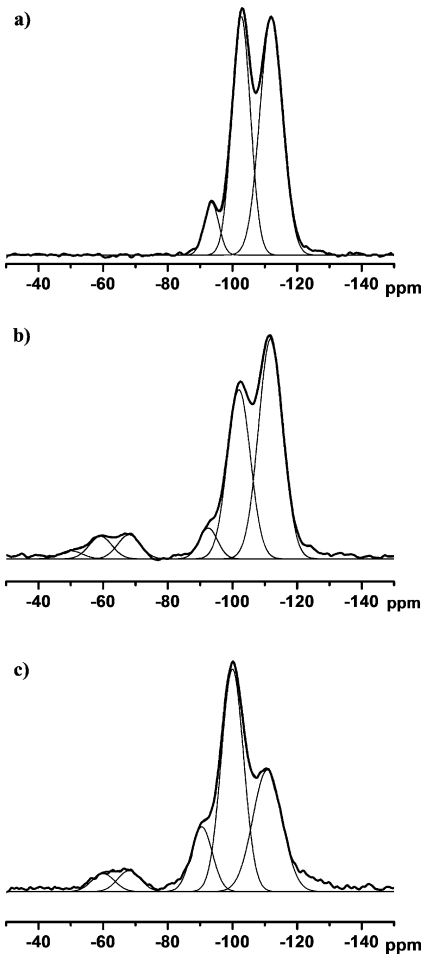

Figure 4. ^{29}Si NMR spectra (400 MHz) recorded at 298 K of the solids a) MCM-4, b) **SNH_2**, and c) **SNH_2-2**.

Table 3. ^{29}Si NMR spectroscopic data for the solids MCM-41, **SNH_2**, and **SNH_2-2** in [%].

	Q^2	Q^3	Q^4	T^1	T^2	T^3
MCM-41	7.3	41.7	51.0	–	–	–
SNH_2	5.2	35.2	48.5	1.6	4.6	4.9
SNH_2-2	12.7	46.2	32.9	–	3.8	4.4

favor of Q^4 (fully condensed) sites was observed in **SNH_2** compared with the MCM-41 material. This variation was in accordance with the appearance of the T^1, T^2, and T^3 peaks corresponding to the anchored silane groups. However, taking into account that each 3-(aminopropyl)triethoxysilane moiety is anchored through at least one silanol group, if not two or three, to guarantee a certain anchoring effect, we could roughly estimate that the decrease in the number of silanol groups was somewhat lower than the incorporation of organosilane groups. Hence, a certain degree of condensation among the incorporated organosilane groups cannot be excluded in addition to their simultaneous anchoring on the silica surface. If there is condensation of silane groups, these species will be located predominantly at the mesopore entrances. Finally, after the second preparative step leading to **SNH_2-2**, there was appreciable hydroxylation of the silica surface, affecting both the Q and T sites. Hence, while the T^3 and T^2 sites were largely preserved, the preparative conditions appear to favor the leaching of T^1-type organosilane groups.

Dye release studies in the presence of explosives

In order to test the proposed sensing mechanism (Scheme 1), the interactions of **SN_3-1**, **SNH_2-2**, and **SN_3-3** with selected explosives were studied on the basis of release of the ruthenium complex entrapped in the porous network of the inorganic supports. Release studies were carried out in acetonitrile solutions, in which tight pore closure was observed and in which both the ruthenium dye and the studied explosives are freely soluble. The following molecules were selected for this study: 2,4-dinitrotoluene (DNT), 2,4,6-trinitrotoluene (TNT), 2,4,6-trinitrophenylmethylnitramine (Tetryl), trinitrobenzene (TNB), hexahydro-1,3,5-trinitro-1,3,5-triazine (RDX), pentaerythritol tetranitrate (PETN), picric acid (PA), triacetone triperoxide (TATP), *N*-methylaniline (NM), 2-nitrotoluene (NT), and nitrobenzene (NB).

In a typical assay, 4 mg of the corresponding solid (**SN_3-1**, **SNH_2-2**, or **SN_3-3**) were suspended in acetonitrile (10 mL) in the presence of DNT, TNT, Tetryl, TNB, RDX, PETN, PA, TATP, NM, NT, or NB (2.0×10^{-3} mol L^{-1}) at 25 °C. Release of the [Ru(bipy)$_3$]$^{2+}$ complex to the bulk solution was easily detected by monitoring its d-π metal-to-ligand charge-transfer (MLCT) transition band at 453 nm or its luminescence at 615 nm (λ_{ex} = 453 nm).[41] As an illustrative example, Figure 5 shows the release kinetics of the ruthenium dye from **SN_3-3** in the presence of selected explosives. As can be seen, solid **SN_3-3** was tightly capped in solution and showed negligible release of the entrapped [Ru(bipy)$_3$]$^{2+}$ complex. The presence of Tetryl, TNT, or

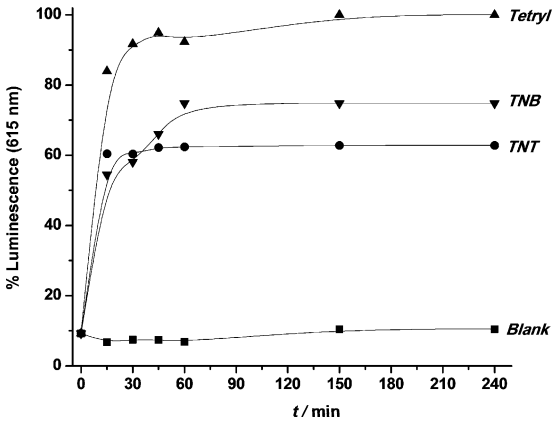

Figure 5. Kinetics of the release of the [Ru(bipy)$_3$]$^{2+}$ dye from solid **SN_3-3** in the absence (blank) and presence of the nitroaromatic explosives Tetryl, TNT, and TNB (2.0×10^{-3} mol L^{-1}) in acetonitrile.

TNB induced opening of the pores and subsequent release of the dye. After around 60 min, the release reached a plateau. In contrast, DNT, RDX, PETN, PA, TATP, NM, NT, and NB were unable to induce release of the ruthenium complex (data not shown) when added to suspensions of probe **SN_3-3**.

Dye release studies on solids **SN_3-1** and **SNH_2-2** gave similar overall results, that is, a tight capping of the pores in the solid alone and release of the dye in the presence of certain explosives. As a summary of the release behavior, Figure 6 shows the relative releases of ruthenium complex from suspensions of solids **SN_3-1**, **SNH_2-2**, and **SN_3-3** in acetonitrile after around 60 min following the addition of different species. As can be seen, Tetryl, TNT, and TNB were able to induce some degree of opening of the "molecular gate" in the three solids with subsequent dye release and *turn-on* of the emission, whereas the other substances tested were unable to induce payload release. **SN_3-3** proved to be a less selective material, with Tetryl, TNT, and TNB inducing almost the same behavior. On the other hand, solid **SNH_2-2** showed a fairly selective response to Tetryl. The studies showed that changes in the nature of the appended TTF derivatives (different sizes and numbers of sulfur atoms) ultimately gave rise to subtle differences in the responses of the three sensing materials.

The above studies demonstrated that **SN_3-1**, **SNH_2-2**, and **SN_3-3** were firmly capped when suspended in acetonitrile. This could be attributed to the formation of dense TTF networks through π-stacking face-to-face and S···S interactions around the pores, which inhibited cargo release. Semiempirical molecular calculations using HyperChem software showed that the anchored TTF derivatives had significant dipole moments of around 1.8, 3.9, and 6.4 D for **1**, **2**, and **3**, respectively. Therefore, it is indeed likely that there will be strong dipole–dipole interactions between anchored molecules around the pore outlets, creating a barrier that inhibits dye release.

When certain nitroaromatic explosives are added to suspensions of the sensing solids, however, the cargo is clearly released. This behavior can most likely be attributed to the formation of TTF–nitroaromatic complexes, which results in rupture of the TTF–TTF interactions (including π-stacking and

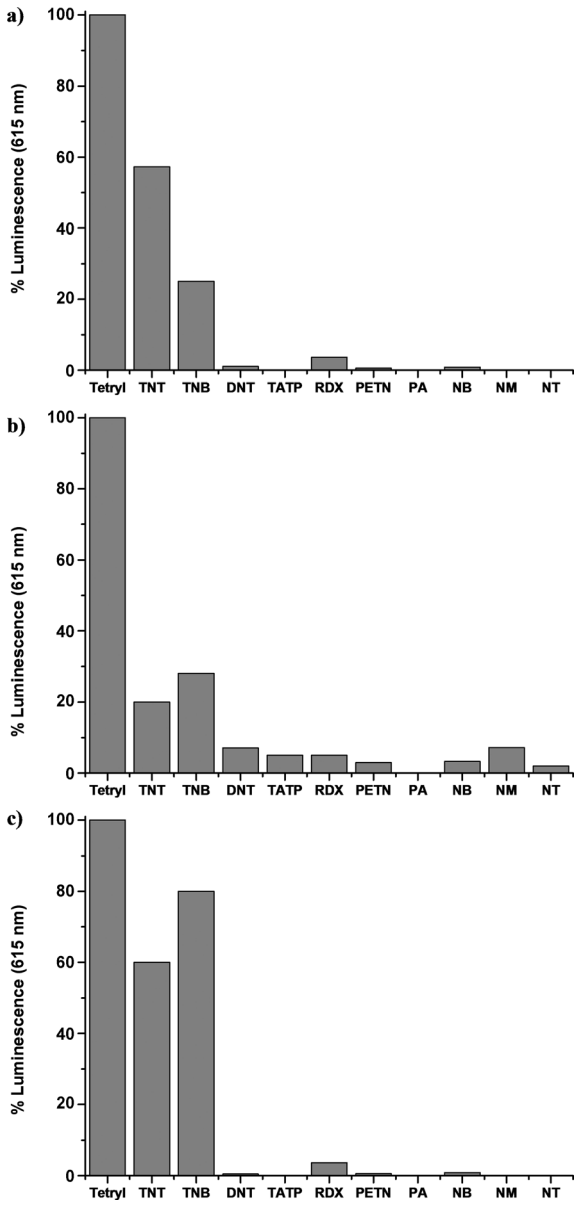

Figure 6. Release of the ruthenium complex from suspensions in acetonitrile of the solids a) **SN_3-1**, b) **SNH_2-2**, and c) **SN_3-3** in the presence of different explosives (2×10^{-3} mol L^{-1}). The emission at 615 nm (excitation at 453 nm) was measured 60 min after addition of the explosive.

dipole interactions), allowing the gate to open. Moreover, this behavior was only observed for molecules displaying strong electron-accepting character, that is, Tetryl, TNT, and TNB, an observation that suggests that it is their interaction with the electron-donating TTF units that is responsible for the uncapping process. Furthermore, ^{13}C MAS NMR spectroscopic investigations carried out on the solids **SN_3** and **SN_3-1** in the presence of Tetryl supported the proposed pore-opening mechanism. Solid **SN_3** showed two well-defined zones in its ^{13}C spectrum, one in the region $\delta = 20$–60 ppm, corresponding to the resonances of the carbon atoms of the propyl chain linking the azido moiety to the inorganic scaffold, and another in the region $\delta = 120$–160 ppm, corresponding to the signals of the bipyridine moieties of the entrapped dye. A ^{13}C MAS NMR spectrum of the final solid **SN_3-1** showed the same two well-defined zones, with the signals of the propyl carbon atoms in the region $\delta = 20$–60 ppm and those of the aromatic carbon atoms in the region $\delta = 120$–170 ppm. The formation of the 1,2,3-triazole ring (due to the "click" reaction) with concomitant immobilization of the TTF moiety resulted in the appearance of new carbon resonances at $\delta = 122.2$, 122.9, 129.4, 137.4, 155.7, 161.6, and 162.8 ppm. In a further experiment, the solid **SN_3-1** was suspended in acetonitrile and an excess of Tetryl was added. The mixture was stirred for 24 h in order to achieve the maximum TTF–Tetryl interaction and concomitant release of the $[Ru(bipy)_3]^{2+}$ complex. The most remarkable feature of the ^{13}C MAS NMR spectrum recorded for this solid was a broadening and small downfield shifts ($\Delta\delta = 0.1$–0.2 ppm) of the TTF signals ($\delta = 120$–170 ppm), which we tentatively attribute to the formation of TTF–Tetryl charge-transfer complexes. In addition, the UV/Vis diffuse-reflectance spectrum (see the Supporting Information) of a mixture of **SN_3-1** and Tetryl in acetonitrile, recorded after 60 min, revealed a slight increase in the reflectance at around 650 nm, which we again tentatively attribute to charge-transfer interactions between the TTF moieties in **SN_3-1** and Tetryl.[20b]

To complete the characterization of the sensing behavior of the hybrid solids **SN_3-1**, **SNH_2-2**, and **SN_3-3**, the limits of detection (LODs) in the presence of TNT, TNB, and Tetryl were determined from the corresponding calibration curves using fluorescence as the detection method (see Table 4). As an example, Figure 7 shows the calibration curve obtained for **SNH_2-2** upon addition of increasing quantities of TNB. LODs for TNT, TNB,

Table 4. Limits of detection in [ppm] for Tetryl, TNT, and TNB using solids **SN_3-1**, **SNH_2-2**, and **SN_3-3**.

Solid	Tetryl	TNT	TNB
SN_3-1	1	6	10
SNH_2-2	1	2	2
SN_3-3	2	7	6

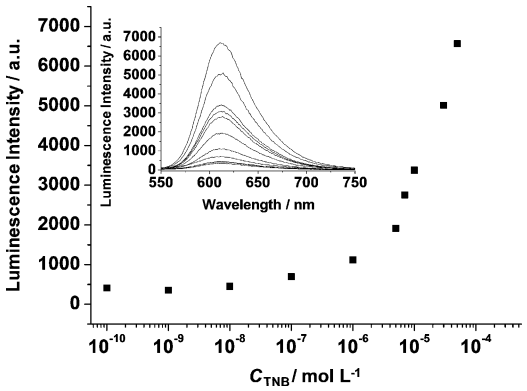

Figure 7. Calibration curve obtained from suspensions in acetonitrile of **SNH_2-2** upon addition of increasing quantities of TNB ($\lambda_{ex} = 453$ nm, $\lambda_{em} = 615$ nm), measuring at 60 min after the addition of TNB. The inset shows the *turn-on* emission spectra of the $[Ru(bipy)_3]^{2+}$ dye released from **SNH_2-2** upon addition of increasing quantities of TNB.

and Tetryl were found to be in the range 1–10 ppm. These values are similar to those found for molecular-based probes,[20] but are higher than those obtained with gold nanoparticles,[42] organic polymers,[43] and tin oxide printed electrodes.[44] A noteworthy distinction, however, is that solids **SN_3-1**, **SNH_2-2**, and **SN_3-3** display a *turn-on* response to nitroaromatic explosives, as opposed to the more common *turn-off* behavior seen with other sensing systems.

Tetryl detection in soils

The obtained LODs (see Table 4) were relatively low and suggested that it might be possible to use the capped solids **SN_3-1**, **SNH_2-2**, and **SN_3-3** to detect explosives within the maximum permissible limits in certain samples. In this context, for instance, the EPA (U.S. Environmental Protection Agency) has stipulated values of 19 μg TNT g^{-1} for residential soil and 79 μg TNT g^{-1} for industrial soil as safety guidelines.[45] After assessing the selective responses of solids **SN_3-1**, **SNH_2-2**, and **SN_3-3** to nitroaromatic explosives in solution, we focused our interest on the possible use of these materials for the detection of explosives in soil samples. For this purpose, we selected solids **SN_3-1** and **SNH_2-2** as sensing systems and Tetryl as a representative explosive. In a typical experiment, 10 g of a finely ground homogeneous soil sample was doped with a known amount of Tetryl (10 mL of a 1.0×10^{-4} mol dm^{-3} Tetryl solution in acetonitrile). The prepared Tetryl-spiked soil sample was then extracted with acetonitrile (3×15 mL). The obtained extracts were combined and concentrated, and the concentrate was redissolved in acetonitrile (10 mL). Five different samples (each 2 mL of the crude extract) were prepared with the addition of increasing volumes of a standard Tetryl solution in acetonitrile, and the final volume of each sample was adjusted to 10 mL by adding the requisite volumes of acetonitrile. Finally, **SN_3-1** or **SNH_2-2** (4 mg) was added to each 10 mL sample solution and the mixtures were stirred for 60 min. Each mixture was then filtered and the absorbance at 453 nm was measured. The well-known standard addition method was followed to calculate the Tetryl concentration. Linear regression analysis was performed, and the slope and *y*-intercept of the calibration curve were used to calculate the concentration of Tetryl in the sample. From the linear regression $A = m\cdot C_{added} + b$, values of $b = 0.04408$ and $m = 46.78$ were obtained, with $R^2 = 0.96$ for solid **SN_3-1**. For **SNH_2-2**, values of $b = 0.1279$, $m = 59.11$, and $R^2 = 0.91$ were obtained. Concentrations of 25.2 μg Tetryl g^{-1} soil using **SN_3-1** and 27.4 μg Tetryl g^{-1} soil using **SNH_2-2** were obtained. These values were in good agreement with the doped concentration (28.7 μg Tetryl g^{-1} soil).

Conclusion

We have reported herein the preparation of three new mesoporous silica supports capped with different electron-donating TTF moieties (**SN_3-1**, **SNH_2-2**, and **SN_3-3**) for a simple chromofluorogenic sensing of nitroaromatic explosives. These materials consist of a mesoporous MCM-41-like structure loaded with a $[Ru(bipy)_3]^{2+}$ complex and capped with TTF derivatives **1**, **2**, and **3**. The capping TTF units (**1** and **3**) used for the preparation of the **SN_3-1** and **SN_3-3** sensory materials were grafted through a "click" chemistry reaction, whereas **SNH_2-2** was functionalized through an amidation reaction with TTF derivative **2**. The three novel materials showed "zero release" when suspended in acetonitrile. Subtle differences in the chemical structures of the TTF capping moieties resulted in different responses of the solids. The explosives Tetryl, TNT, and TNB were found to be capable of inducing, to some extent, dye release from **SN_3-1** and **SN_3-3**, whereas solid **SNH_2-2** showed a fairly selective response to Tetryl. Most notably, a *turn-on* response was observed. All other substances tested were unable to induce payload release. Moreover, color or emission measurement revealed that detection of Tetryl, TNB, and TNT at the ppm level could be achieved. Finally, **SN_3-1** and **SNH_2-2** have been used for the chromogenic detection of Tetryl in soil samples with good results. The principle of this method is amenable to various modifications. For instance, the support, the π-donor units, and the dye may be easily changed without the use of complex chemistry in order to tune the selectivity and the optical properties of the signaling dye.

Experimental Section

Caution! Explosives should be used with extreme caution and handled only in small quantities.

General methods

Powder X-ray diffraction, thermogravimetric (TG) analysis, and N_2 adsorption–desorption techniques were used to characterize the prepared materials. X-ray measurements were carried out on a Philips D8 Advance diffractometer using CuKα radiation. TG analyses were carried out on a TGA/SDTA 851e Mettler Toledo balance under an oxidizing atmosphere (air, 80 mL min^{-1}) with a heating program consisting of a heating ramp of 10 K per minute from 293 K to 1273 K and an isothermal heating step at this temperature of duration 30 min. N_2 adsorption–desorption isotherms were recorded with a Micromeritics ASAP2010 automated sorption analyzer. Samples were degassed at 393 K in vacuum overnight. Specific surface areas were calculated from the adsorption data in the low-pressure range using the Brunauer–Emmett–Teller (BET) model. Pore size was determined according to the Barrett–Joyner–Halenda (BJH) method. TEM images were obtained with a Philips CM10 microscope operating at 100 kV. UV/Vis spectra were measured at 298 K on a Perkin–Elmer Lambda 35 UV/Vis spectrophotometer. Fluorescence spectroscopy studies were carried out at 298 K with JASCO FP-8500 and Felix 32 Analysis, version 1.2 (Build 56) PTI (Photon Technology International) spectrofluorimeters. 1D and 2D NMR spectra were obtained on a Bruker AVANCE III 400 MHz spectrometer; ^{1}H NMR spectra were recorded at 400 MHz at 298 K and ^{13}C NMR spectra were recorded at 100 MHz at 298 K. Samples for NMR analysis were dissolved in deuterated solvents purchased from Cambridge Isotope Laboratories or Sigma–Aldrich, and TMS or the residual solvent was used as an internal standard. ^{29}Si and ^{13}C MAS NMR spectra were recorded on a Bruker WB AVANCE III 400 MHz spectrometer operating at 79.5 and 128.3 MHz, respectively, with a magic-angle spinning speed of 10 kHz. Electron impact ionization mass spectrometry (EI-MS) was performed on a Thermo Finnigan MAT SSQ710 single-stage quadrupole instrument. Matrix-assisted laser-desorption/ionization mass spectrome-

try was performed on a Bruker Autoflex III Smartbeam mass spectrometer, utilizing a 2,5-dihydroxybenzoic acid (DHB) matrix. In order to estimate the dipole moments of the grafted TTF derivatives (products **1**, **2**, and **3**), quantum chemical calculations were carried out at the semi-empirical level with HyperChem 6.03 software (HyperChem 6.03 Molecular Modeling System, Hypercube Inc., Gainesville, Florida, USA, 2000).

Chemicals

Tetraethyl orthosilicate (TEOS; 98%), *n*-cetyltrimethylammonium bromide (CTAB; $\geq$ 99%), sodium hydroxide ($\geq$ 98%), triethanolamine ($TEAH_3$; $\geq$ 99%), tris(2,2′-bipyridyl)dichlororuthenium(II) hexahydrate ($[Ru(bipy)_3]Cl_2{\cdot}6H_2O$; 100%), 2,4-dinitrotoluene (DNT), *N*-methylaniline (NM; 98%), 2-nitrotoluene (NT), nitrobenzene (NB; 99%), picric acid (PA), tetrathiafulvalene (TTF), perfluorohexyl iodide (PFHI), lithium diisopropylamide (LDA), potassium fluoride (KF), ethynyltrimethylsilane, tetrakis(palladium)triphenylphosphine ($Pd(PPh_3)_4$), mercury(II) acetate, acetic acid, Celite 545, CH_2Cl_2, $NaHCO_3$, $MgSO_4$, triethyl phosphate, toluene, diethyl ether, petroleum ether, LiBr, dimethyl sulfoxide (DMSO), MeOH, sodium methoxide, CuI, K_3PO_4, $LiOH{\cdot}H_2O$, oxalyl chloride, tetra-*n*-butylammonium fluoride, (±)-*trans*-1,2-diaminocyclohexane, pyridine, 3-(aminopropyl)triethoxysilane, and tetrahydrofuran (THF) were provided by Sigma–Aldrich and were used as received. The nitroaromatic explosives 2,4,6-trinitrophenylmethylnitramine (Tetryl), 2,4,6-trinitrotoluene (TNT), 1,3,5-trinitrobenzene (TNB), hexahydro-1,3,5-trinitro-1,3,5-triazine (RDX), pentaerythritol tetranitrate (PETN), and 3-(azidopropyl)triethoxysilane were purchased as 3% solutions in acetonitrile from SelectLab Chemicals. Triacetone triperoxide (TATP),[46] 4,5-bis(butylthio)-1,3-dithiole-2-thione[35] (**3a**), and *N*-tosyl-1,3-dithiolo[4,5-*c*]pyrrole-2-one[36] (**3b**) were synthesized according to literature procedures. L-Ascorbic acid sodium salt (99%), potassium carbonate, sodium sulfate, and copper(II) sulfate pentahydrate ($CuSO_4{\cdot}5H_2O$) were acquired from Scharlab (Barcelona, Spain). Diisopropylamine (iPr_2NH) was acquired from Fluka. Analytical grade solvents were purchased from Scharlab (Barcelona, Spain). All reagents were used as received, except for THF, which was distilled from sodium/benzophenone prior to use.

Mesoporous MCM-41 microparticles

The molar ratio of the reagents in the mother liquor was fixed at 7.0 $TEAH_3$: 2.0 TEOS : 0:52 CTAB : 0.50 NaOH : 8.89 H_2O. The mesoporous MCM-41 support was first synthesized according to the so-called "atrane route", in which CTAB (4.68 g) was added to a solution of $TEAH_3$ (25.79 g) containing a silatrane derivative (TEOS; 11 mL, 0.049 mol) at 118 °C. Next, water (80 mL) was slowly added with vigorous stirring at 70 °C. After a few minutes, a white suspension was formed. This mixture was aged at room temperature overnight. The resulting powder was collected by filtration and washed with water and ethanol until the washings were of pH 6–7. Finally, the white solid was dried at 70 °C (as-synthesized MCM-41). To prepare the final porous material, the as-synthesized solid was calcined at 550 °C under an oxidizing atmosphere for 5 h in order to remove the template phase (MCM-41).

Solid SN_3-1

In a typical synthesis, template-free MCM-41 (1 g) and $[Ru(bipy)_3]Cl_2{\cdot}6H_2O$ (0.6 g, 0.8 mmol) were suspended in acetonitrile (40 mL) in a round-bottomed flask. To remove the adsorbed water, 10 mL of acetonitrile was distilled off using a Dean–Stark set-up. The mixture was then stirred for 24 h at room temperature to fully load the pores of the MCM-41 scaffold. An excess of 3-(azidopropyl)triethoxysilane (0.49 mL, 2 mmol) was then added to the reaction mixture, and the suspension was stirred for 5.5 h. Thereafter, the orange-yellow solid was collected by filtration to afford $\mathbf{SN_3}$. Meanwhile, anhydrous DMF (50 mL) was purged with N_2 for 1 h and the TTF derivative **1** (121.1 mg, 0.531 mmol) was placed in an empty flask. Using a needle, an aliquot of the N_2-purged DMF (10 mL) was transferred into the flask containing **1**. A similar procedure was used for a mixture of ascorbic acid (56.3 mg, 0.32 mmol) and $CuSO_4{\cdot}5H_2O$ (39.9 mg, 0.16 mmol). Thereafter, solid $\mathbf{SN_3}$ was suspended in DMF/water (1:2, v/v) containing $[Ru(bipy)_3]Cl_2{\cdot}6H_2O$ (0.6 g, 0.8 mmol). The ascorbic acid/$CuSO_4{\cdot}5H_2O$ solution in anhydrous DMF was then added to the reaction mixture by means of a needle. Finally, a similar operation was carried out with the solution of the TTF derivative **1** in DMF. After the additions were completed, the reaction mixture was stirred at room temperature for 5 days. Thereafter, the resulting microparticles were collected by filtration, washed with CH_2Cl_2 (100 mL), water (100 mL), acetonitrile (100 mL), and THF (100 mL), and dried at 35 °C for 12 h to afford $\mathbf{SN_3}$**-1** (872 mg) as a green-brown solid.

Solid SNH_2-2

In a typical synthesis, template-free MCM-41 (1 g) and $[Ru(bipy)_3]Cl_2{\cdot}6H_2O$ (0.6 g, 0.8 mmol) were suspended in acetonitrile (40 mL) in a round-bottomed flask. To remove the adsorbed water, 10 mL of acetonitrile was distilled off using a Dean–Stark set-up. The mixture was then stirred for 24 h at room temperature to fully load the pores of the MCM-41 scaffold. An excess of 3-(aminopropyl)triethoxysilane (0.47 mL, 2 mmol) was then added, and the suspension was stirred for 5.5 h. The resulting orange-yellow solid was collected by filtration to afford $\mathbf{SNH_2}$. Subsequently, $\mathbf{SNH_2}$ (1 g) was suspended in acetonitrile (40 mL) and compound **2** (378.3 mg, 1.06 mmol), the ruthenium dye (600 mg, 0.8 mmol), and K_2CO_3 (2 g, 14.5 mmol) were added. The resulting suspension was heated under reflux for 16 h under an inert atmosphere of argon. Finally, the solid $\mathbf{SNH_2}$ was collected by filtration, extensively washed with water and thereafter with a mixture of acetonitrile and water (100 mL of acetonitrile and 100 mL of milli-Q water per 100 mg of final solid, stirring for 24 h) before being dried overnight at 36 °C to afford $\mathbf{SNH_2}$**-2** (1.98 g) as a brown solid.

5-Tosyl-2-[4,5-bis(butylthio)-1,3-dithiol-2-ylidene]-[1,3]dithiolo[4,5-*c*]pyrrole (3c)

The thione **3a** (4.00 g, 12.8 mmol) and the ketone **3b** (3.36 g, 10.79 mmol) were dissolved in freshly distilled triethyl phosphite (60 mL) and the mixture was degassed under an argon atmosphere for 15 min. The reaction mixture was quickly heated to 130 °C. After 16 min at 130 °C, another portion of the thione **3a** (4.00 g, 12.8 mmol) was added and the reaction mixture was stirred at 130 °C for 1.2 h, then cooled to room temperature. Cold methanol (75 mL) was added and the resulting orange solid was collected by filtration. The filtrate was left in a freezer overnight to produce a second crop of the product, which was collected by filtration. The combined solids were washed with small portions of methanol (5×15 mL) and dried in vacuo before being purified by flash chromatography (SiO_2; CH_2Cl_2/petroleum ether, 1:1, as eluent). The yellow band (R_f = 0.29, CH_2Cl_2/petroleum ether, 1:1) was collected and concentrated to give the title compound **3c** (5.25 g, 85%) as yellow crystals.[47] ^{1}H NMR (500 MHz, $(CD_3)_2SO$): δ = 0.86 (t, J = 7.3 Hz, 6H), 1.31–1.43 (m, 4H), 1.47–1.57 (m, 4H), 2.38 (s, 3H), 2.84 (t, J = 7.3 Hz, 4H), 6.94 (s, 2H), 7.30 (d, J = 8.6 Hz, 2H), 7.73 ppm (d, J = 8.6 Hz, 2H); ^{13}C NMR (125 MHz, $(CD_3)_2SO$): δ = 13.5, 20.9, 21.1,

31.3, 35.1, 112.4, 112.7, 117.4, 125.9, 126.7, 126.8, 130.4, 134.5, 145.8 ppm; MS (MALDI): *m/z*: calcd for $C_{23}H_{27}NO_2S_7^+$: 573.01; found: 572.98.

2-[4,5-Bis(butylthio)-1,3-dithiol-2-ylidene]-[1,3]dithiolo[4,5-*c*]pyrrole (3 d)

Compound **3 c** (4.46 g, 7.77 mmol) was dissolved in a mixture of anhydrous THF (250 mL) and methanol (100 mL) and the mixture was degassed under an argon atmosphere for 60 min. Sodium methoxide (25% w/w in MeOH, 4.323 g, 80.03 mmol) was added in one portion and the reaction mixture was heated under reflux for 30 min. After allowing the mixture to cool to room temperature, water (400 mL) was added, and the resulting mixture was extracted with CH_2Cl_2 (2×200 mL). The combined organic phases were dried ($MgSO_4$) and concentrated to give a yellow oil, which was purified by flash chromatography (SiO_2; CH_2Cl_2/cyclohexane, 2:1, gradient elution). The broad yellow band was collected and concentrated to afford the title compound **3 d** (2.90 g, 89%) as a yellow powder.[47] ^{1}H NMR (500 MHz, $(CD_3)_2SO$): $\delta = 0.87$ (t, $J = 7.3$ Hz, 6H), 1.35–1.42 (m, 4H), 1.49–1.59 (m, 4H), 2.85 (t, $J = 7.3$ Hz, 4H), 6.81 (s, 2H), 11.14 ppm (br s, 1H); ^{13}C NMR (125 MHz, $(CD_3)_2SO$): $\delta = 13.5$, 20.9, 31.31, 35.0, 107.4, 110.8, 117.1, 121.7, 126.7 ppm; MS (MALDI): *m/z*: calcd for $C_{16}H_{21}NS_6^+$: 419.00; found: 418.98.

2-[4,5-Bis(butylthio)-1,3-dithiol-2-ylidene]-5-{4-[(trimethylsilyl)ethynyl]phenyl}-[1,3]dithiolo[4,5-*c*]pyrrole (3 f)

Compound **3 d** (1.05 g, 2.502 mmol), CuI (0.93 g, 4.878 mmol), K_3PO_4 (1.78 g, 8.388 mmol), and (4-iodophenylethynyl)trimethylsilane (**3 e**) (3.60 g, 12.0 mmol) were dissolved in freshly distilled THF (50 mL) and the mixture was degassed under an argon atmosphere for 20 min, and then (±)-*trans*-1,2-diaminocyclohexane (1.06 g, 1.2 mL, 9.33 mmol) was added in one portion. The mixture was heated at 115 °C in a microwave oven for 3 h, then allowed to cool to room temperature and extracted with CH_2Cl_2 (100 mL). The organic phase was washed with aqueous NaOH solution (5% in 100 mL H_2O; 3×20 mL) and water (3×150 mL), and then dried ($MgSO_4$). Concentration gave a yellow residue, which was purified by column chromatography (SiO_2; CH_2Cl_2/petroleum ether, 1:3, gradient elution). The yellow band ($R_f = 0.74$, CH_2Cl_2/petroleum ether, 1:1) was collected and concentrated to provide the title compound **3 f** (0.99 g, 68%) as yellow crystals. M.p. 116.0–118.0 °C; ^{1}H NMR (500 MHz, CD_2Cl_2): $\delta = 0.25$ (s, 9H), 0.92 (t, $J = 7.3$ Hz, 6H), 1.40–1.48 (m, 4H), 1.59–1.65 (m, 4H), 2.84 (t, $J = 7.3$ Hz, 4H), 6.94 (s, 2H), 7.28 (d, $J = 8.8$ Hz, 2H), 7.50 ppm (d, $J = 8.8$ Hz, 2H); ^{13}C NMR (125 MHz, CD_2Cl_2): $\delta = 0.1$, 13.9, 22.2, 32.4, 36.5, 95.6, 104.4, 111.2, 119.9, 121.2, 123.3, 128.2, 133.9, 140.3 ppm (two signals are missing/overlapping); HRMS-EI: *m/z*: calcd for $C_{27}H_{33}NS_6Si^+$: 591.0701; found: 591.1000; elemental analysis calcd (%) for $C_{27}H_{33}NS_6Si$ (592.0): C 54.78, H 5.62, N 2.37; found: C 54.97, H 5.80, N 2.38.

2-[4,5-Bis(butylthio)-1,3-dithiol-2-ylidene]-5-(4-ethynylphenyl)-[1,3]dithiolo[4,5-*c*]pyrrole (3)

Compound **3 f** (0.30 g, 0.5 mmol) was dissolved in anhydrous THF (10 mL) and then tetra-*n*-butylammonium fluoride (0.26 g, 1 mmol) was added in one portion. The reaction mixture was stirred for 20 min at room temperature, then diluted with water (75 mL) and extracted with CH_2Cl_2 (2×75 mL). The combined organic phases were dried ($MgSO_4$) and concentrated to afford the title compound **3** (0.25 g, 99%) as an analytically pure orange solid. M.p. 165.8–137.2 °C; ^{1}H NMR (500 MHz, $(CD_3)_2SO$): $\delta = 0.88$ (t, $J = 7.3$ Hz, 6H), 1.37–1.43 (m, 4H), 1.52–1.58 (m, 4H), 2.87 (t, $J = 7.3$ Hz, 4H), 4.23 (s, 1H), 7.53 (s, 2H), 7.55 ppm (s, 4H); ^{13}C NMR (125 MHz, $(CD_3)_2SO$): $\delta = 13.3$, 20.8, 31.1, 34.9, 81.1, 82.7, 109.6, 111.3, 118.5, 121.4, 126.6, 133.1, 139.2 ppm (two signals are missing/overlapping); HRMS-EI: *m/z*: calcd for $C_{24}H_{25}NS_6^+$: 519.0306; found: 518.9600; elemental analysis calcd (%) for $C_{24}H_{25}NS_6$ (519.9): C 55.45, H 4.85, N 2.69; found: C 55.38, H 4.89, N 2.80.

Solid SN_3-3

In a typical synthesis, template-free MCM-41 (1 g) and $[Ru(bipy)_3]Cl_2 \cdot 6H_2O$ (0.6 g, 0.8 mmol) were suspended in acetonitrile (40 mL) in a round-bottomed flask. To remove the adsorbed water, 10 mL of acetonitrile was distilled off using a Dean–Stark set-up. The mixture was then stirred for 24 h at room temperature to fully load the pores of the MCM-41 scaffold. An excess of 3-(azidopropyl)triethoxysilane (1.20 mL, 5 mmol) was then added, and the suspension was stirred for 5.5 h. The resulting orange-yellow solid was collected by filtration and washed with CH_2Cl_2 (50 mL) to afford **SN_3**. Subsequently a mixture of **SN_3** (0.5 g) and compound **3** (303.2 mg, 0.98 mmol) was suspended in DMF/water (1:1, v/v, 40 mL) in the presence of an excess of the ruthenium(II) dye (0.3 g, 0.4 mmol) (in order to avoid release of the dye from the pores to the bulk solution during the synthesis of this solid). Finally, a solution of $CuSO_4 \cdot 5H_2O$ (1.248 mg, 0.005 mmol) and sodium ascorbate (9.905 mg, 0.05 mmol) was added and the reaction mixture was stirred at room temperature for 5 days. The microparticles were collected by filtration and extensively washed with water and then with acetonitrile (100 mL of acetonitrile per 100 mg of final solid, stirring for 24 h), and finally dried at 36 °C for 12 h to afford **SN_3-3** as a yellow solid (0.55 g).

Acknowledgements

Financial support from the Spanish Government (project MAT2012–38429-C04–01) and the Generalitat Valencia (project PROMETEO/2009/016) is gratefully acknowledged. J. O. Jeppesen gratefully acknowledges financial support provided by the EC FP7 ITN "FUNMOLS" Project No. 212942), the Villum Foundation, the Carlsberg Foundation, and the Danish Natural Science Research Council (#11–106744). Y. Salinas thanks the Spanish Ministry of Science and Innovation for her grant. We also thank Stephen Boyer, School of Human Sciences, Science Centre, London Metropolitan University, for carrying out the elemental analyses.

Keywords: gated materials · mesoporous materials · nitroaromatic explosives · optical detection · sensors · tetrathiafulvalene

[1] a) S. Singh, *J. Hazard. Mater.* **2007**, *144*, 15–28; b) R. Schulte-Ladbeck, M. Vogel, U. Karst, *Anal. Bioanal. Chem.* **2006**, *386*, 559–565; c) R. G. Smith, N. D'Souza, S. Nicklin, *Analyst* **2008**, *133*, 571–584.
[2] J. P. Agrawal, R. D. Hodgson, *Organic Chemistry of Explosives*, Wiley, Chichester, **2007**.
[3] K. S. Focsaneanu, J. C. Scaiano, *Photochem. Photobiol. Sci.* **2005**, *4*, 817–821.
[4] K. G. Furton, L. J. Myers, *Talanta* **2001**, *54*, 487–500.
[5] K. Hakansson, R. V. Coorey, R. A. Zubarev, V. L. Talrose, P. Hakansson, *J. Mass Spectrom.* **2000**, *35*, 337–346.
[6] M. E. Walsh, *Talanta* **2001**, *54*, 427–438.
[7] J. M. Sylvia, J. A. Janni, J. D. Klein, K. M. Spencer, *Anal. Chem.* **2000**, *72*, 5834–5840.

[8] a) J. Yinon, *Mass Spectrom. Rev.* **1982**, *1*, 257 – 307; b) J. C. Mathurin, T. Faye, A. Brunot, J. C. Tabet, *Anal. Chem.* **2000**, *72*, 5055 – 5062.
[9] S. F. Hallowell, *Talanta* **2001**, *54*, 447 – 458.
[10] C. Vourvopoulos, P. C. Womble, *Talanta* **2001**, *54*, 459 – 468.
[11] A. M. O'Mahony, J. Wang, *Anal. Methods* **2013**, *5*, 4296 – 4309.
[12] E. Wallis, T. M. Griffin, N. Popkie Jr. , M. A. Eagan, R. F. McAtee, D. Vrazel, J. McKinly, *Proc. SPIE-Int. Soc. Opt. Eng.* **2005**, *5795*, 54 – 64.
[13] Y. Salinas, R. Martínez-Máñez, M. D. Marcos, F. Sancenón, A. M. Costero, M. Parra, S. Gil, *Chem. Soc. Rev.* **2012**, *41*, 1261 – 1296.
[14] M. E. Germain, M. J. Knapp, *Chem. Soc. Rev.* **2009**, *38*, 2543 – 2555.
[15] a) H. Kong, B. J. Jung, J. Sinha, H. E. Katz, *Chem. Mater.* **2012**, *24*, 2621 – 2623; b) P. Frere, P. J. Skabara, *Chem. Soc. Rev.* **2005**, *34*, 69 – 98.
[16] See, for instance: a) Y. Salinas, E. Climent, R. Martínez-Máñez, F. Sancenón, M. D. Marcos, J. Soto, A. M. Costero, S. Gil, M. Parra, A. Pérez de Diego, *Chem. Commun.* **2011**, *47*, 11885 – 11887; b) Y. Salinas, A. Agostini, E. Pérez-Esteve, R. Martínez-Máñez, F. Sancenón, M. D. Marcos, J. Soto, A. M. Costero, S. Gil, M. Parra, P. Amorós, *J. Mater. Chem. A* **2013**, *1*, 3561 – 3564; c) Y. Salinas, R. Martínez-Máñez, J. O. Jeppesen, L. H. Petersen, F. Sancenón, M. D. Marcos, J. Soto, C. Guillem, P. Amorós, *ACS Appl. Mater. Interfaces* **2013**, *5*, 1538 – 1543.
[17] See, for example: a) A. D. Hughes, I. C. Glenn, A. D. Patrick, A. Ellington, E. V. Anslyn, *Chem. Eur. J.* **2008**, *14*, 1822 – 1827; b) Y. H. Lee, H. Liu, J. Y. Lee, S. H. Kim, S. K. Kim, J. L. Sessler, Y. Kim, J. S. Kim, *Chem. Eur. J.* **2010**, *16*, 5895 – 5901; c) C. Vijayakumar, G. Tobin, W. Schmitt, M. Kima, M. Takeuchi, *Chem. Commun.* **2010**, *46*, 874 – 876; d) G. V. Zyryanov, M. A. Palacios, P. Anzembacher Jr. , *Org. Lett.* **2008**, *10*, 3681 – 3684.
[18] a) J. O. Jeppesen, M. B. Nielsen, J. Becher, *Chem. Rev.* **2004**, *104*, 5115 – 5132; b) F. Wudl, D. Wobschal, E. J. Hufnagel, *J. Am. Chem. Soc.* **1972**, *94*, 670 – 672; c) J. Ferraris, V. Walatka, J. Perlstein, D. O. Cowan, *J. Am. Chem. Soc.* **1973**, *95*, 948 – 949.
[19] a) M. Adam, K. Müllen, *Adv. Mater.* **1994**, *6*, 439 – 459; b) T. Jørgensen, T. K. Hansen, J. Becher, *Chem. Soc. Rev.* **1994**, *23*, 41 – 51; c) M. R. Bryce, *J. Mater. Chem.* **1995**, *5*, 1481 – 1496; d) J. Garían, *Adv. Heterocycl. Chem.* **1995**, *62*, 249 – 304; e) G. Schukat, E. Fanghänel, *Sulfur Rep.* **1996**, *18*, 1 – 294; f) M. R. Bryce, *J. Mater. Chem.* **2000**, *10*, 589 – 598; g) M. B. Nielsen, C. Lomholt, J. Becher, *Chem. Soc. Rev.* **2000**, *29*, 153 – 164; h) J. L. Segura, N. Martín, *Angew. Chem.* **2001**, *113*, 1416 – 1455; *Angew. Chem. Int. Ed.* **2001**, *40*, 1372 – 1409.
[20] a) D. S. Kim, V. M. Lynch, K. A. Nielsen, C. Johnsen, J. O. Jeppesen, J. L. Sessler, *Anal. Bioanal. Chem.* **2009**, *395*, 393 – 400; b) K. A. Nielsen, W.-S. Cho, J. O. Jeppesen, V. M. Lynch, J. Becher, J. L. Sessler, *J. Am. Chem. Soc.* **2004**, *126*, 16296 – 16297; c) J. Su Park, F. Le Derf, C. M. Bejger, V. M. Lynch, J. L. Sessler, K. A. Nielsen, C. Johnsen, J. O. Jeppesen, *Chem. Eur. J.* **2010**, *16*, 848 – 854.
[21] a) A. B. Descalzo, R. Martínez-Máñez, F. Sancenón, K. Hoffmann, K. Rurack, *Angew. Chem.* **2006**, *118*, 6068 – 6093; *Angew. Chem. Int. Ed.* **2006**, *45*, 5924 – 5948; b) K. Ariga, A. Vinu, J. P. Hill, T. Mori, *Coord. Chem. Rev.* **2007**, *251*, 2562 – 2591.
[22] See, for example: a) E. Aznar, R. Martínez-Máñez, F. Sancenón, *Expert Opin. Drug Delivery* **2009**, *6*, 643 – 655; b) B. G. Trewyn, I. I. Slowing, S. Giri, H. T. Chen, V. S. Y. Lin, *Acc. Chem. Res.* **2007**, *40*, 846 – 853; c) S. Saha, K. C. F. Leung, T. D. Nguyen, J. F. Stoddart, J. I. Zink, *Adv. Funct. Mater.* **2007**, *17*, 685 – 693; d) R. Klajn, J. F. Stoddart, B. A. Grzybowski, *Chem. Soc. Rev.* **2010**, *39*, 2203 – 2237.
[23] a) J. S. Beck, J. C. Vartuli, W. J. Roth, M. E. Leonowicz, C. T. Kresge, K. D. Schmitt, C. T. W. Chu, D. H. Olson, E. W. Sheppard, S. B. McCullen, J. B. Hoggins, J. L. Schlenker, *J. Am. Chem. Soc.* **1992**, *114*, 10834 – 10843; b) A. P. Wight, M. E. Davis, *Chem. Rev.* **2002**, *102*, 3589 – 3614; c) G. Kickelbick, *Angew. Chem.* **2004**, *116*, 3164 – 3166; *Angew. Chem. Int. Ed.* **2004**, *43*, 3102 – 3104; d) K. Ariga, A. Vinu, Y. Yamauchi, Q. Ji, J. P. Hill, *Bull. Chem. Soc. Japan* **2012**, *85*, 1 – 32.
[24] See, for example: a) N. K. Mal, M. Fujiwara, Y. Tanaka, *Nature* **2003**, *421*, 350 – 353; b) E. Aznar, L. Mondragón, J. V. Ros-Lis, F. Sancenón, M. D. Marcos, R. Martínez-Máñez, J. Soto, E. Pérez-Payá, P. Amorós, *Angew. Chem.* **2011**, *123*, 11368 – 11371; *Angew. Chem. Int. Ed.* **2011**, *50*, 11172 – 11175; c) C. Chen, J. Geng, F. Pu, X. Yang, J. Ren, X. Qu, *Angew. Chem.* **2011**, *123*, 912 – 916; *Angew. Chem. Int. Ed.* **2011**, *50*, 882 – 886; d) E. Ruíz-Hernández, A. Baeza, M. Valler-Regí, *ACS Nano* **2011**, *5*, 1259 – 1266; e) E. Bringas, O. Köysüeren, D. V. Quach, M. Mahmoudi, E. Aznar, J. D. Roehling, M. D. Marcos, R. Martínez-Máñez, P. Stroeve, *Chem. Commun.* **2012**, *48*, 5647 – 5649; f) A. Agostini, F. Sancenón, R. Martínez-Máñez, M. D. Marcos, J. Soto, P. Amorós, *Chem. Eur. J.* **2012**, *18*, 12218 – 12221.
[25] See, for example: a) N. Mas, I. Galiana, L. Mondragón, E. Aznar, E. Climent, N. Cabedo, F. Sancenón, J.-R. Murguía, R. Martínez-Máñez, M. D. Marcos, P. Amorós, *Chem. Eur. J.* **2013**, *19*, 11167 – 11171; b) H. Meng, M. Xue, T. Xia, Y. L. Zhao, F. Tamanoi, J. F. Stoddart, J. I. Zink, A. E. Nel, *J. Am. Chem. Soc.* **2010**, *132*, 12690 – 12697; c) A. Schlossbauer, C. Dohmen, D. Schaffert, E. Wagner, T. Bein, *Angew. Chem.* **2011**, *123*, 6960 – 6962; *Angew. Chem. Int. Ed.* **2011**, *50*, 6828 – 6830; d) M. Chen, C. Huang, C. He, W. Zhu, Y. Xu, Y. Lu, *Chem. Commun.* **2012**, *48*, 9522 – 9524; e) R. Hernandez, H. R. Tseng, J. W. Wong, J. F. Stoddart, J. I. Zink, *J. Am. Chem. Soc.* **2004**, *126*, 3370 – 3371; f) E. Aznar, R. Villalonga, C. Giménez, F. Sancenón, M. D. Marcos, R. Martínez-Máñez, P. Díez, J. M. Pingarrón, P. Amorós, *Chem. Commun.* **2013**, *49*, 6391 – 6393.
[26] See, for instance: a) A. Schlossbauer, J. Kecht, T. Bein, *Angew. Chem.* **2009**, *121*, 3138 – 3141; *Angew. Chem. Int. Ed.* **2009**, *48*, 3092 – 3095; b) C. Park, H. Kim, S. Kim, C. Kim, *J. Am. Chem. Soc.* **2009**, *131*, 16614 – 16615; c) P. D. Thornton, A. Heise, *J. Am. Chem. Soc.* **2010**, *132*, 2024 – 2028; d) A. Agostini, L. Mondragón, C. Coll, E. Aznar, M. D. Marcos, R. Martínez-Máñez, F. Sancenón, J. Soto, E. Pérez-Payá, P. Amorós, *ChemistryOpen* **2012**, *1*, 17 – 20; e) A. Bernardos, L. Mondragón, I. Javakhishvili, N. Mas, C. de La Torre, R. Martínez-Máñez, F. Sancenón, J. M. Barat, S. Hvilsted, M. Orzaez, E. Pérez-Payá, P. Amorós, *Chem. Eur. J.* **2012**, *18*, 13068 – 13078; f) A. Agostini, L. Mondragón, A. Bernardos, R. Martínez-Máñez, M. D. Marcos, F. Sancenón, J. Soto, A. Costero, C. Manguan-García, R. Perona, M. Moreno-Torres, R. Aparicio-Sanchis, J. R. Murguía, *Angew. Chem. Int. Ed.* **2012**, *51*, 10556 – 10560; g) I. Candel, E. Aznar, L. Mondragón, C. de La Torre, R. Martínez-Máñez, F. Sancenón, M. D. Marcos, P. Amorós, C. Guillem, E. Pérez-Payá, A. Costero, S. Gil, M. Parra, *Nanoscale* **2012**, *4*, 7237 – 7245; h) A. Agostini, L. Mondragón, L. Pascual, E. Aznar, C. Coll, R. Martínez-Máñez, F. Sancenón, J. Soto, M. D. Marcos, P. Amorós, A. M. Costero, M. Parra, S. Gil, *Langmuir* **2012**, *28*, 14766 – 14776.
[27] a) R. Casasús, E. Aznar, M. D. Marcos, R. Martínez-Máñez, F. Sancenón, J. Soto, P. Amorós, *Angew. Chem.* **2006**, *118*, 6813 – 6816; *Angew. Chem. Int. Ed.* **2006**, *45*, 6661 – 6664; b) C. Coll, R. Casasús, E. Aznar, M. D. Marcos, R. Martínez-Máñez, F. Sancenón, J. Soto, P. Amorós, *Chem. Commun.* **2007**, 1957 – 1959; c) E. Aznar, C. Coll, M. D. Marcos, R. Martínez-Máñez, F. Sancenón, J. Soto, P. Amorós, J. Cano, E. Ruíz, *Chem. Eur. J.* **2009**, *15*, 6877 – 6888; d) E. Climent, R. Martínez-Máñez, F. Sancenón, M. D. Marcos, J. Soto, A. Maquieira, P. Amorós, *Angew. Chem.* **2010**, *122*, 7439 – 7441; *Angew. Chem. Int. Ed.* **2010**, *49*, 7281 – 7283; e) E. Climent, L. Mondragón, R. Martínez-Máñez, F. Sancenón, M. D. Marcos, J. R. Murguía, P. Amorós, K. Rurack, E. Pérez-Payá, *Angew. Chem.* **2013**, *125*, 9106 – 9110; *Angew. Chem. Int. Ed.* **2013**, *52*, 8938 – 8942; f) Y. Zhang, Q. Yuan, T. Chen, X. Zhang, Y. Chen, W. Tan, *Anal. Chem.* **2012**, *84*, 1956 – 1962; g) R. Qian, L. Ding, H. Ju, *J. Am. Chem. Soc.* **2013**, *135*, 13282 – 13285; h) M. Oroval, E. Climent, C. Coll, R. Eritja, A. Aviñó, M. D. Marcos, F. Sancenón, R. Martínez-Máñez, P. Amorós, *Chem. Commun.* **2013**, *49*, 5480 – 5482; i) E. Climent, A. Bernardos, R. Martínez-Máñez, A. Maquieira, M. D. Marcos, N. Pastor-Navarro, R. Puchades, F. Sancenón, J. Soto, P. Amorós, *J. Am. Chem. Soc.* **2009**, *131*, 14075 – 14080; j) E. Climent, R. Martínez-Máñez, A. Maquieira, F. Sancenón, M. D. Marcos, E. M. Brun, J. Soto, P. Amorós, *ChemistryOpen* **2012**, *1*, 251 – 259; k) E. Climent, D. Gröninger, M. Hecht, M. A. Walter, R. Martínez-Máñez, M. G. Weller, F. Sancenón, P. Amorós, K. Rurack, *Chem. Eur. J.* **2013**, *19*, 4117 – 4122.
[28] R. Martínez-Máñez, F. Sancenón, M. Hencht, M. Biyical, K. Rurack, *Anal. Bioanal. Chem.* **2011**, *399*, 55 – 74.
[29] a) E. Climent, M. D. Marcos, R. Martínez-Máñez, F. Sancenón, J. Soto, K. Rurack, P. Amorós, *Angew. Chem.* **2009**, *121*, 8671 – 8674; *Angew. Chem. Int. Ed.* **2009**, *48*, 8519 – 8522; b) M. Hecht, E. Climent, M. Biyikal, F. Sancenón, R. Martínez-Máñez, K. Rurack, *Coord. Chem. Rev.* **2013**, *257*, 2589 – 2606.
[30] C. Coll, A. Bernardos, R. Martínez-Máñez, F. Sancenón, *Acc. Chem. Res.* **2013**, *46*, 339 – 349.
[31] S. Cabrera, J. El Haskouri, C. Guillem, J. Latorre, A. Beltrán, D. Beltrán, M. D. Marcos, P. Amorós, *Solid State Sci.* **2000**, *2*, 405 – 420.
[32] H. C. Kolb, M. G. Finn, K. B. Sharpless, *Angew. Chem.* **2001**, *113*, 2056 – 2075; *Angew. Chem. Int. Ed.* **2001**, *40*, 2004 – 2021.

[33] a) C. Goze, S. X. Liu, C. Leiggener, L. Sanguinet, E. Levillain, A. Hauser, S. Decurtins, *Tetrahedron* **2008**, *64*, 1345 – 1350; b) T. Otsubo, Y. Koichi, A. Bitoh, F. Oruga, *Chem. Lett.* **1994**, 2047 – 2050.
[34] a) K. Heuzé, M. Foumigue, P. Batail, *J. Mater. Chem.* **1999**, *9*, 2373 – 2379; b) P. Blanchard, M. Sallé, G. Duguay, M. Jubault, A. Gorgues, *Tetrahedron Lett.* **1992**, *33*, 2685 – 2688.
[35] a) N. Le Narvor, N. Robertson, E. Wallace, J. D. Kilburn, A. E. Underhill, N. P. Bartlett, M. Webster, *J. Chem. Soc., Dalton Trans.* **1996**, 823 – 828; b) T. Chen, C. Wang, Z. Cong, B. Ying, K. Imafuku, *Heterocycles* **2005**, *65*, 187 – 193.
[36] a) J. O. Jeppesen, K. Takimiya, N. Thorup, J. Becher, *Synthesis* **1999**, 803 – 810; b) J. O. Jeppesen, K. Takimiya, F. Jensen, T. Brimert, K. Nielsen, N. Thorup, J. Becher, *J. Org. Chem.* **2000**, *65*, 5794 – 5805.
[37] C. Cai, A. Vasella, *Helv. Chim. Acta* **1995**, *78*, 732 – 757.
[38] E. P. Barrett, L. G. Joyner, P. P. Halenda, *J. Am. Chem. Soc.* **1951**, *73*, 373 – 380.
[39] S. Brunauer, P. H. Emmett, E. Teller, *J. Am. Chem. Soc.* **1938**, *60*, 309 – 319.
[40] R. Casasús, E. Climent, M. D. Marcos, R. Martínez-Mañez, F. Sancenón, J. Soto, P. Amorós, J. Cano, E. Ruiz, *J. Am. Chem. Soc.* **2008**, *130*, 1903 – 1917.
[41] a) F. Felix, J. Ferguson, H. U. Gudel, A. Ludi, *J. Am. Chem. Soc.* **1980**, *102*, 4096 – 4102; b) F. E. Lytle, D. M. Hercules, *J. Am. Chem. Soc.* **1969**, *91*, 253 – 257.
[42] Y. Jiang, H. Zhao, N. Zhu, Y. Lin, P. Yu, L. Mao, *Angew. Chem.* **2008**, *120*, 8729 – 8732; *Angew. Chem. Int. Ed.* **2008**, *47*, 8601 – 8604.
[43] S. W. Thomas III, G. D. Joly, T. M. Swager, *Chem. Rev.* **2007**, *107*, 1339 – 1386.
[44] E. S. Forzani, D. Lu, M. J. Leright, A. Díaz Aguilar, F. Tsow, R. A. Iglesias, Q. Zhang, J. Lu, J. Li, N. Tao, *J. Am. Chem. Soc.* **2009**, *131*, 1390 – 1391.
[45] EPA Technical Fact Sheet: 2,4,6-Trinitrotoluene (TNT), May **2012**.
[46] D. F. Laine, C. W. Roske, I. F. Cheng, *Anal. Chim. Acta* **2008**, *608*, 56 – 60.
[47] M. Takase, N. Yoshida, T. Nishinaga, M. Iyoda, *Org. Lett.* **2011**, *13*, 3896 – 3899.

Received: June 26, 2013
Revised: October 10, 2013
Published online on December 6, 2013